



Article

Numerical Analysis of NO_x Reduction Using Ammonia Injection and Comparison with Water Injection

María Isabel Lamas Galdo ^{1,*}, Laura Castro-Santos ¹ and Carlos G. Rodríguez Vidal ²¹ Escola Politécnica Superior, Universidade da Coruña, 15403 Ferrol, Spain; laura.castro.santos@udc.es² Norplan Engineering S.L., 15570 Naron, Spain; c.rodriguez.vidal@udc.es

* Correspondence: isabel.lamas.galdo@udc.es; Tel.: +34-881013896

Received: 8 January 2020; Accepted: 7 February 2020; Published: 11 February 2020



Abstract: This work analyzes NO_x reduction in a marine diesel engine using ammonia injection directly into the cylinder and compares this procedure with water injection. A numerical model based on the so-called inert species method was applied. It was verified that ammonia injection can provide almost 80% NO_x reduction for the conditions analyzed. Furthermore, it was found that the effectiveness of the chemical effect using ammonia is extremely dependent on the injection timing. The optimum NO_x reduction was obtained when ammonia is injected during the expansion stroke, while the optimum injection timing using water is near top dead center. Chemical, thermal, and dilution effects of both ammonia and water injection were compared. The chemical effect was dominant in the case of ammonia injection. On the other hand, water injection reduces NO_x through dilution and, more significantly, through a thermal effect.

Keywords: CFD; NO_x; engine; ammonia; water injection

1. Introduction

Nowadays, diesel engines rule the transportation sector and power most of the ships in the world. These engines are efficient compared with other thermal machines but emit harmful species such as nitrogen oxides (NO_x), soot, carbon dioxide (CO₂), sulfur oxides (SO_x), carbon monoxide (CO), and non-burnt hydrocarbons (HC). Between these, NO_x is a harmful component that must be reduced since it produces acidification of rain, photochemical smog, greenhouse effects, ozone depletion, and respiratory diseases. Several international, national, and regional policies have been developed to limit NO_x and other pollutants. In the marine field, the European Commission and the Environmental Protection Agency limit emissions in the European Union and the United States, respectively. On an international level, the International Maritime Organization (IMO) maintains a comprehensive regulatory framework for shipping. In 1973, the IMO adopted Marpol 73/78, the International Convention for the Prevention of Pollution from Ships, designed to reduce marine pollution. In particular, Marpol Annex VI limits NO_x emissions for marine ships depending on the manufacturing data, engine speed, and working geographical area.

Due to these increasingly restrictive regulations, several NO_x reduction methods have been developed in recent years. One of them is the utilization of alternative fuels. The main alternative marine fuels may be found in two forms: liquid fuels including ethanol, methanol, bio-liquid fuel, and biodiesel; and gaseous fuels, including propane, hydrogen, and natural gas [1–4].

Operating under diesel, there are two procedures to reduce NO_x, which are primary and secondary measures. The former reduces the amount of NO_x during combustion, while the latter focuses on removing NO_x from the exhaust gases through downstream cleaning techniques. It is well known

that the main factors that influence NO_x formation are the temperatures reached in the combustion process and the amount of time in which the combustion gases remain at high temperatures [5–7]. Based on this, primary measures focus on addressing these factors and reducing the concentrations of oxygen and nitrogen [8,9]. Well-known primary measures are exhaust gas recirculation (EGR), Miller timing, common rail, modification of injection and other parameters of the engine, and water addition. Water can be introduced as a fuel-water emulsion injected via the fuel valve, through separate nozzles or by humidifying the scavenge air. Despite the extensive research on primary measures along the recent years, a procedure to reduce NO_x without decreasing emission of other pollutants and/or consumption has not effectively been developed. In this regard, secondary measures reduce NO_x from the flue gas through downstream cleaning techniques. Many applications have been undertaken to reduce NO_x by selective catalytic reduction (SCR) and selective non-catalytic reduction (SNCR). The disadvantages of SCR are its price, poor durability of catalysts, and deposition of particulate on the catalyst. These disadvantages are not present in SNCR, but this procedure is limited to a narrow temperature range with optimal temperatures that are much higher than those characteristic of flue gas from diesel engines [10]. This limitation constitutes a drawback for practical applications in exhaust gases from diesel engines. As SCR reducing agents, ammonia (NH_3), urea, and cyanuric acid have been extensively employed. SNCR using ammonia, urea, and cyanuric acid are known as De NO_x [11,12], NO_xOUT [13,14], and RAPRENO [15–17], respectively. Between these, this work focuses on NO_x reduction using ammonia. The NO_x reduction capabilities of ammonia were discovered in the seventies by Lyon [18], who found that ammonia selectively reduces NO_x without a catalyst over the temperature range of 1100–1400 K. Typical exhaust gas temperatures from marine engines, around 300–450 °C [19], remain considerably lower than this optimal temperature range for NO_x reduction. Comprehensive investigations have been reported about SNCR analyzing parameters such as temperature, the molar ratio (NH_3/NO) [20], residence time, oxygen level, initial NO_x , combustibles, and so on [21,22], verifying that the most important factor for NO_x reduction is the temperature. Based on this result, Miyamoto et al. [23] proposed to reduce NO_x emissions by injecting ammonia or urea directly into the cylinder. They found an optimum NO_x reduction at injection timing 90° CA ATDC (crankshaft angle after top dead center), i.e., during the expansion stroke, under temperatures between 1100–1600 K. Nam and Gibbs [24] analyzed direct injection of urea and ammonia using a flow reactor which simulates a single cylinder diesel engine, while Nam and Gibbs [25] analyzed the influence of injection temperature, the molar ratio NH_3/NO , residence time, and combustion products, focusing on kinetic parameters. Larbi and Bessrouer [26] developed an analytical model to analyze ammonia injection and concluded that the temperature and thus injection timing is critical. In fact, if ammonia is injected near TDC (top dead center), it performs as a fuel instead of as a NO_x reducing agent, since ammonia can also be employed as a fuel [27,28].

These aforementioned studies delivered interesting knowledge about ammonia injection, but an experimental analysis cannot provide complete information about the governing effects. In this regard, Computational Fluid Dynamics (CFD) offers an alternative method to analyze the performance and emissions on engines. In the field of medium and large marine engines, CFD is especially useful because an experimental setup is extremely expensive and a downscale model sometimes is not accurate enough. In particular, the so-called artificial inert species method allows us to investigate several chemical and physical effects separately. This method was initiated by Guo [29], who used an artificial inert component with the same properties as hydrogen to analyze the chemical, dilution and thermal effects of hydrogen addition on a HCCI engine. Voshtani et al. [30] and Neshat et al. [31] analyzed these chemical, dilution, and thermal effects on a blended fuel of isooctane and n-heptane. Subsequently, they studied these effects on reformer gas addition [32] and water addition [33].

This work presents a CFD analysis to study NO_x reduction in a commercial marine engine, the Wärtsilä 6 L 46. The NO_x reduction procedure is based on ammonia injection during the expansion stroke. The artificial inert species method was applied to characterize thermal, dilution and chemical effects of ammonia injection. In addition, ammonia injection was compared with water (H_2O) injection.

2. Materials and Methods

This section describes the engine analyzed and the numerical model employed to study the performance and emissions.

2.1. Description of the Engine Analyzed

As mentioned above, the engine analyzed is the Wärtsilä 6 L 46 (Wärtsilä Corporation, Finland) [34,35], diesel, six-cylinder, four-stroke, water-cooled, and turbocharged. Each cylinder of this engine has two intake and two exhaust valves and a fuel injector with 20 holes is situated at the center of the cylinder head. This is a direct injection engine, i.e., the fuel is injected directly into the cylinder. The injection pump provides injection pressures up to 1500 bar. Optionally, this engine includes the possibility to incorporate direct water injection (DWI) to incorporate water at 400 bar from an external pump unit to each injection. The injector is thus equipped with a dual nozzle with separate needles for water and fuel. This system was employed in the numerical model to simulate water or ammonia injection.

In the present work, a comprehensive analysis was performed in a Wärtsilä 6 L 46 installed on a tuna fishing vessel. Many parameters were characterized at different loads, such as in-cylinder pressure, consumption, indicated and effective power, scavenging air pressure and temperature, exhaust gas pressure and temperature, lubricating oil pressure and temperature, cooling water temperature, emissions, etc. Although this engine is designed to operate under heavy fuel oil, marine diesel oil operation is also possible. Since these data were taken on board and near the coast, marine diesel oil was employed. The viscosity and density of this fuel are $12.5 \text{ mm}^2/\text{s}$ and $885 \text{ kg}/\text{m}^3$ at $15 \text{ }^\circ\text{C}$ and its sulfur content 0.89%. For instance, Figure 1 indicates the results of the in-cylinder pressure along the operating cycle, at 100% load. The engine performance analyzer MALIN 6000 was employed to characterize the in-cylinder pressure. This pressure transducer is connected to the bleed valve, located at the engine head, which acts as an indicator channel. It worth mentioning that the experimental pressure trace can be distorted due to pressure waves in the channel [36], and that no algorithm was applied to correct this drawback.

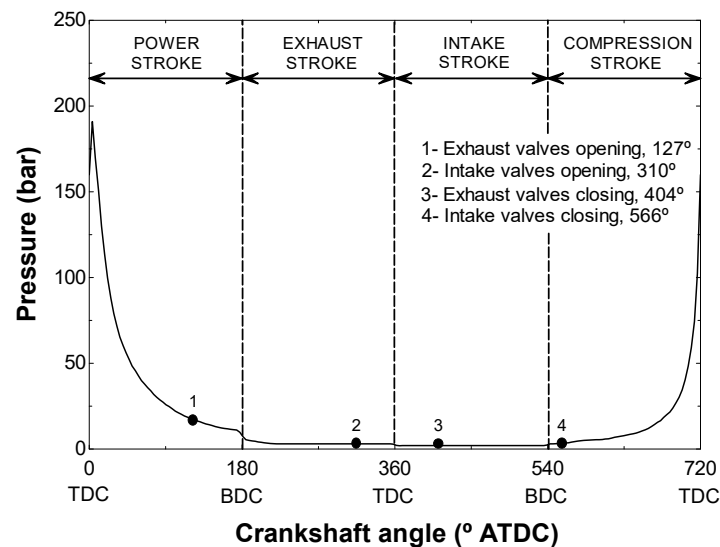


Figure 1. In-cylinder pressure at 100% load, experimentally measured.

Other experimental data at different loads are indicated in Table 1. In particular, the speed, power, mean indicated pressure (MIP), maximum pressure, specific fuel consumption (SFC), and emissions. NO_x , CO, HC, and CO_2 emissions were analyzed using the Gasboard-3000 series (Wuhan Cubic) gas analyzers, particularly Gasboard-3030 for HC and Gasboard-3000 for NO, CO, and CO_2 . The load, speed, and SFOC were taken from the engine monitoring system.

Table 1. Experimental data.

Load (%)	25	35	50	75	100	
Speed (rpm)	500	500	500	500	500	
Power (kW)	2047.6	2367.8	2923.6	4051.1	5430.1	
MIP (bar)	8.1	13.9	17.6	20.0	22.5	
P _{max} (bar)	102.7	138.0	160.4	175.8	182.3	
SFC (g/kWh)	173.2	171.9	169.8	169.5	172.1	
Emissions	NO _x (ppm)	1048	1092	1149	1167	1128
	HC (ppm)	510	485	448	466	515
	CO (ppm)	261	255	247	268	292
	CO ₂ (%)	3.5	4.6	6.9	7.9	8.3

2.2. Numerical Model

The open software OpenFOAM was employed in the present work. The mesh is indicated in Figure 2. In order to implement the movement of the piston and valves, a deforming mesh was used. In particular, Figure 2a represents the tridimensional mesh, Figure 2b a cross-section at BDC (bottom dead center), i.e., 180° or 540° CA ATDC, and Figure 2c a cross-section at TDC, i.e., 0° or 360° CA ATDC. Several meshes with different elements were tested in order to verify that the results are independent of the mesh size. Table 2 indicates the error obtained between experimental and numerical results of pressure and fractions using a mesh with 501,769 elements at BDC (mesh 1), as well as 802,527 (mesh 2) and 1,264,873 (mesh 3). As can be seen, there is no difference between the meshes 2 and 3. For this reason, the mesh 2 was chosen for the present work.

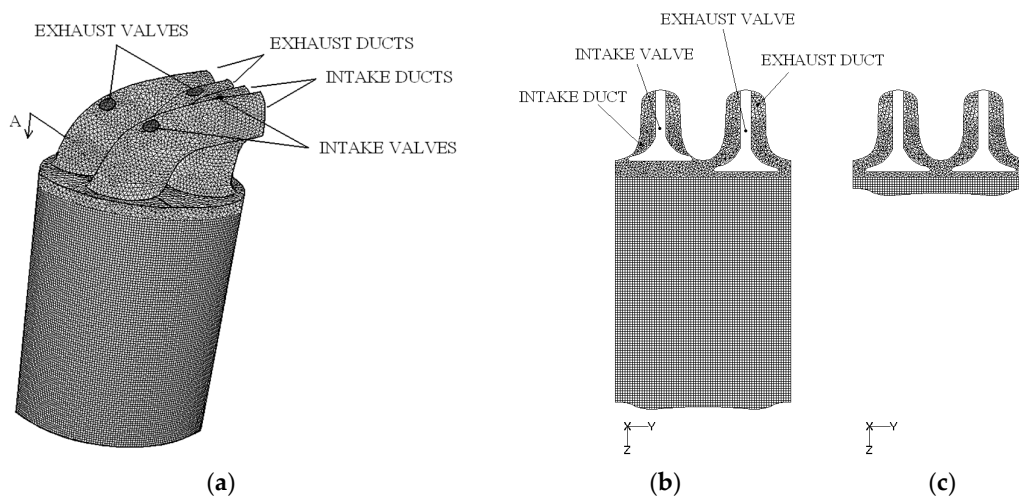


Figure 2. (a) Tridimensional mesh at BDC; (b) Cross-section mesh at BDC; (c) Cross-section mesh at TDC.

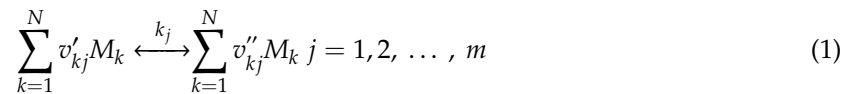
Table 2. Error (%) at 100% load obtained using different mesh sizes.

	P	NO _x	CO	HC	CO ₂
Mesh 1	4.2	5.1	8.1	6.5	4.7
Mesh 2	4.1	4.9	7.9	6.4	4.6
Mesh 3	4.1	4.9	7.9	6.4	4.6

A new in-house solver was programmed using C++. Briefly, this solver is based on the RANS (Reynolds-averaged Navier Stokes) equations of conservation of mass, momentum, and energy. The k-ε turbulence model was chosen.

The standard Kelvin-Helmholtz and Rayleigh-Taylor breakup (KH-RT) model [37] was employed for fuel droplet breakup, and the Dukowicz model [38] for the heat-up and evaporation. A comprehensible analysis about the adequacy of breakup models can be found in the literature. Compared to other breakup models such as WAVE, TAB (Taylor Analogy Breakup), etc., the KH-RT model is more suitable for the high injection pressures that take place in diesel engines [39]. As indicated previously, ammonia and water injection were modeled through an injector equipped with a dual nozzle with separate needles for water/ammonia and fuel.

In order to solve the chemical kinetics, a reaction mechanism was programmed by adding the three kinetic schemes described in Sections 2.1–2.3 for combustion (131 reactions and 41 species), NO_x formation (43 reactions and 20 species) and NO_x reduction (131 reactions and 41 species), respectively. Several additional equations must be added to model chemical kinetics. Given a set of N species and m reactions, Equation (1), the local mass fraction of each species, f_k , can be expressed by using Equation (2).



$$\frac{\partial}{\partial t}(\rho f_k) + \frac{\partial}{\partial x_i}(\rho u_i f_k) = \frac{\partial}{\partial x_i} \left(\frac{\mu_t}{S_{ct}} \frac{\partial f_k}{\partial x_i} \right) + S_k \quad (2)$$

In the equations above, ρ is the density, u the velocity, v'_{kj} the stoichiometric coefficients of the reactant species M_k in the reaction j , v''_{kj} the stoichiometric coefficients of the product species M_k in the reaction j , S_{ct} the turbulent Schmidt number, and S_k the net rate of production of the species M_k by chemical reaction, given by the molecular weight multiplied by the production rate of the species, Equation (3).

$$S_k = MW_k \frac{d[M_k]}{dt} \quad (3)$$

where MW_k is the molecular weight of the species M_k and $[M_k]$ its concentration. The net progress rate is given by the production of the species M_k minus the destruction of the species M_k along the m reactions:

$$\frac{d[M_k]}{dt} = \sum_{j=1}^m \left\{ (v'_{kj} - v''_{kj}) \left[k_{fj} \prod_{k=1}^N [M_k]^{v'_{kj}} - k_{bj} \prod_{k=1}^N [M_k]^{v''_{kj}} \right] \right\} \quad (4)$$

where k_{fj} and k_{bj} are the forward and backward reaction rate constants for each reaction j .

The simulation started at 360° CA ATDC and the whole cycle was analyzed. The initial pressure was 1.31 bar, obtained from experimental measurements. Concerning boundary conditions, the intake valve pressure and temperature after the turbocharger were 2.72 bar and 514 K, respectively. The heat transfer from the cylinder to the cooling water was modeled as a combined convection-radiation type, Equation (5). Previous investigations [40] demonstrated the accuracy of this type of boundary condition in comparison with adiabatic or constant temperature:

$$q = h(T_{gas} - T_{water}) \quad (5)$$

where q is the heat transferred, T_{gas} the in-cylinder temperature, T_{water} the cooling water temperature (78 °C), and h the heat transfer coefficient, given by the following expression [41]:

$$h = 10.4 kb^{-1/4} (u_{piston}/\nu)^{3/4} \quad (6)$$

where b is the cylinder bore, k the thermal conductivity of the gas, u_{piston} the mean piston speed, and ν the kinematic viscosity of the gas. Substituting values into the above equation yields $h = 4151 \text{ W/m}^2\text{K}$.

2.2.1. Combustion Kinetic Scheme

The fuel was treated as n-heptane. The kinetic scheme of Ra and Reitz [42], based on 131 reactions and 41 species, was employed for combustion. Another common approach to treat combustion in CFD is to assume that the kinetics is so fast that chemical species remain at equilibrium due to the high temperatures. Nevertheless, previous works [43,44] indicated that a kinetic scheme is more accurate than the equilibrium hypothesis, since the cooling during the expansion process and dilution with the excess air elongates the time needed to achieve equilibrium. Indeed, several studies about diesel engines verified that the measured CO emissions are higher than those provided by the equilibrium concentrations. The reason is that one of the sources of CO in diesel engines are lean regions which are not able to burn properly [45,46]. This happens when the local turbulent and diffusion time scales are much smaller than the time required to achieve equilibrium. In these cases, the chemical equilibrium hypothesis leads us to overestimate the levels of the minor species. For these reasons, another procedure developed in the present work was the implementation of a chemical kinetic model. Figure 3 represents the CO and HC emissions experimentally and numerically obtained using chemical equilibrium and the kinetic model. As can be seen, the kinetic model improves the results. Regarding CO₂ emissions, these remain practically inalterable so are not included in the figure. According to the improvement obtained using the kinetic model compared to the equilibrium assumption, the kinetic model developed by Ra and Reitz [42] was employed in the remainder of the present work.

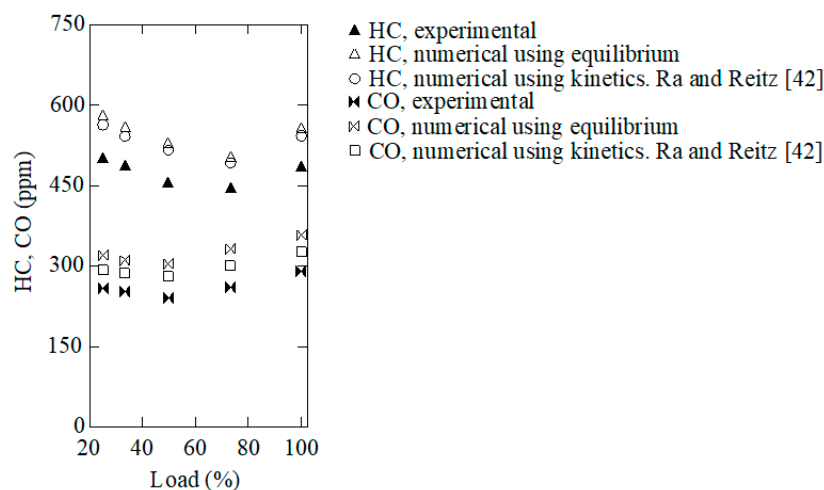


Figure 3. HC and CO emissions experimentally and numerically obtained.

2.2.2. NO_x Formation Kinetic Scheme

The numerical model employs the kinetic scheme of Yang et al. [47], based on 43 reactions and 20 species. In CFD, it is common to employ the so called extended Zeldovich mechanism [48,49], based on 3 reactions and 7 species. Nevertheless, previous works [44,50] compared several kinetic schemes using experimental results and concluded that the model of Yang et al. provides satisfactorily accurate results.

2.2.3. NO_x Reduction Kinetic Scheme

The kinetic scheme chosen for NO_x reduction is the one proposed by Miller and Glarborg [51], based on 134 reactions and 24 species. The accuracy of this and other kinetic schemes was also compared with experimental measurements elsewhere [43,52], concluding that the model of Miller and Glarborg [51] provides satisfactorily accurate results.

2.3. Validation of the Overall Numerical Model

The overall numerical model, summarized in Table 3, was validated using experimental measurements. The emissions and consumption obtained experimentally and numerically at several loads are shown in Figure 4. This figure includes CO, CO₂, NO_x, HC, and SFC. As can be seen, a reasonable correspondence between numerical and experimental results was obtained. The in-cylinder pressure obtained experimentally and numerically at 100% load is shown in Figure 5. This figure also indicates a satisfactory correspondence between experimental and numerical results. Other loads also provided satisfactory concordance between experimental and numerical results, and thus are not represented again.

Table 3. Numerical models.

Turbulence Model	<i>k-ε</i>
Evaporation model	Dukowicz
Breakup model	KH-RT
Combustion model	Ra and Reitz
NO _x formation model	Yang et al.
NO _x reduction model	Miller and Glarborg

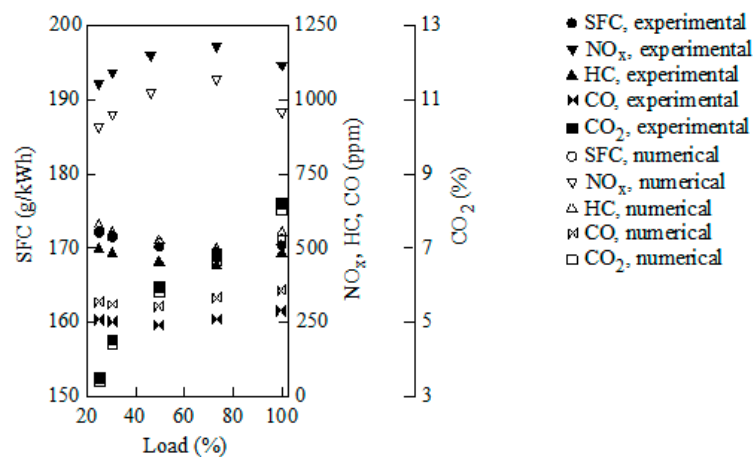


Figure 4. NO_x, HC, CO and CO₂ emissions as well as BSFC experimentally and numerically obtained.

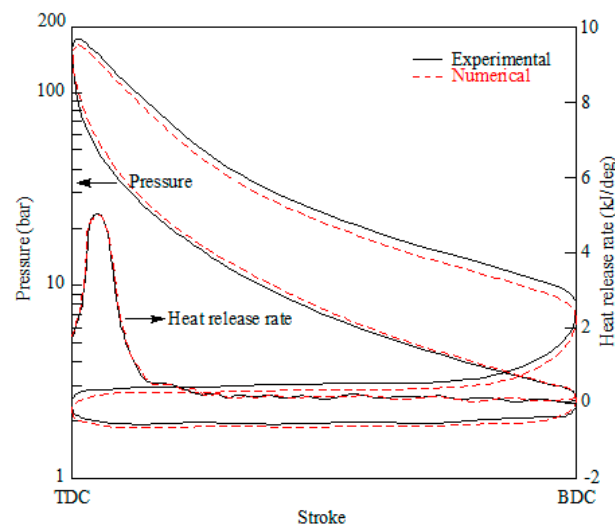


Figure 5. In-cylinder pressure experimentally and numerically obtained at 100% load.

3. Results and Discussion

Once the numerical model was validated, it was employed to analyze NO_x reduction through ammonia and water injection directly into the cylinder. This section presents the results obtained. First of all, results about NO_x reduction are exposed and then results obtained from the artificial inert species method.

3.1. NO_x Reduction

First of all, it is necessary to determine the appropriate quantity of ammonia and water. Regarding ammonia, its main disadvantage is the non-reacted ammonia slip in the exhaust gas. Ammonia is highly toxic, and thus it is important to maintain an un-reacted ammonia slip to the exhaust that is as low as possible. Figure 6 represents the NO_x reduction as well as the ammonia slip in the exhaust gas against the ammonia to fuel ratio, Equation (7), at 100% load. In this figure, the ammonia injection took place 58.4° CA ATDC. This value was chosen because it provides the maximum NO_x reduction, as will be shown below. The effect on CO, HC, and SFC remained practically negligible, so these are not represented in this figure. As can be seen, NO_x reduction improves with the ammonia to fuel ratio, with a tendency to level off around 4%. Ammonia to fuel ratios higher than 3% provide a few additional NO_x reductions with a considerable increment of un-reacted ammonia emitted to the atmosphere, and NO_x reduction drops again for higher ratios since ammonia itself oxidizes to NO. For this reason, an ammonia to fuel ratio of 4% was employed in the remainder of the present work.

$$\text{Ammonia to fuel ratio (\%)} = \frac{\text{mass of ammonia}}{\text{mass of fuel}} 100 \tag{7}$$

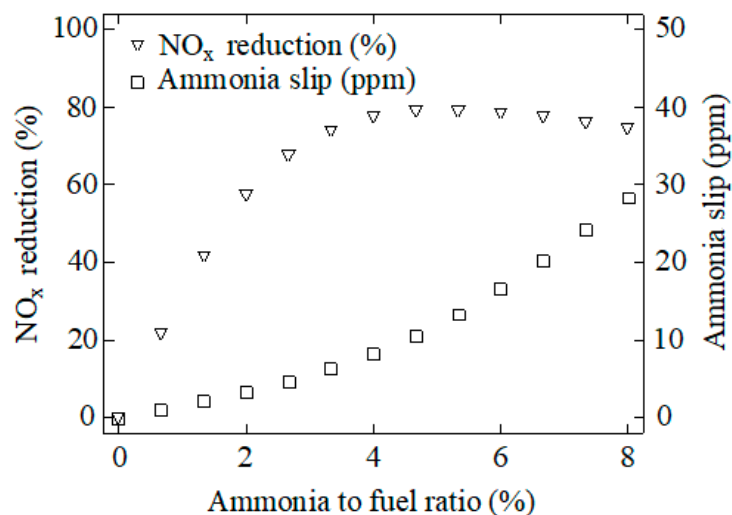


Figure 6. NO_x reduction and ammonia slip against the ammonia to fuel ratio. Ammonia injection timing: 58.4° CA ATDC.

As indicated previously, the present work focuses on water injection through a dual nozzle with separated needles for water and fuel. Using this DWI system, typical water to fuel ratios, Equation (8), in practical applications are within the range 40%–70% [20]. Figure 7 shows the NO_x reduction, as well as the effect on SFC, CO, and HC for water to fuel ratios from 0 to 100% at 100% load. As can be seen in this figure, the water to fuel ratio improves NO_x reduction, but increments both consumption and emissions of CO and HC. For this reason and taking into account usual practical applications, a water to fuel ratio of 70% was employed in the remainder of the present work.

$$\text{Water to fuel ratio (\%)} = \frac{\text{mass of water}}{\text{mass of fuel}} 100 \tag{8}$$

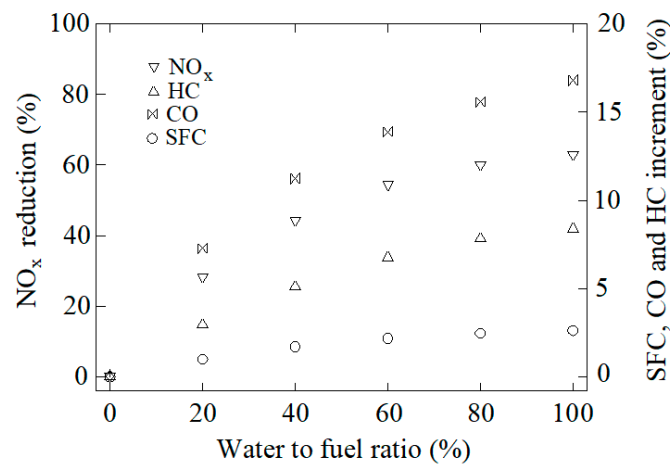


Figure 7. NO_x reduction against the water to fuel ratio. Water injection timing: -2.1° CA ATDC.

Figure 8 shows the effect of the injection timing on NO_x reduction. Ammonia and water were compared using 4% ammonia to fuel ratio and 70% water to fuel ratio. As can be seen in this figure, using water injection a maximum 57.1% NO_x reduction was obtained at -2.1° CA ATDC. On the other hand, if ammonia is injected around TDC, then the NO_x reduction is considerably smaller than when using a water injection. Nevertheless, at 58.4° CA ATDC, NO_x reduction reaches 78.1% using ammonia. As mentioned in the introduction, NO_x reduction using ammonia is very sensitive to the temperature. Injected near TDC, ammonia is not efficient due to the excessive in-cylinder temperatures. Nevertheless, at 58.4° CA ATDC, the in-cylinder temperatures reduce to the optimal values required for NO_x reduction using ammonia. Instead of 100% loads, at lower loads the in-cylinder temperatures are lower too and thus the optimum injection time takes place before 58.4° CA ATDC.

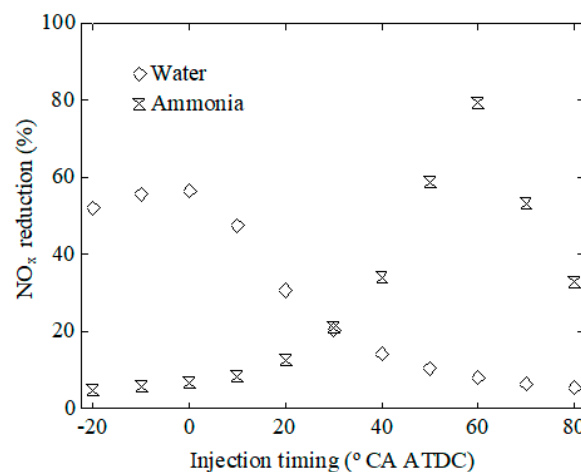


Figure 8. NO_x reduction against the injection timing using ammonia and water. Ammonia to fuel ratio: 4%, water to fuel ratio: 70%.

Figure 9 shows the maximum temperature for the base case without a water or ammonia injection, with a 4% ammonia to fuel ratio and with a 70% water to fuel ratio at 100% load. In these simulations, both ammonia and water were injected at -2.1° CA ATDC. As can be seen, water promotes a reduction in the combustion temperatures. The maximum temperature is lowered 93.2°C if 70% water is injected at -2.1° CA ATDC. On the other hand, ammonia increases the maximum temperature 8.4°C if this is injected at -2.1° CA ATDC. This explains the effect on CO, HC, and SFC. As indicated above, ammonia has a negligible effect on these parameters and water increases them. Water reduces the combustion temperature due to the increment in the specific heat capacity of the cylinder gases (water has higher

specific heat capacity than air) and lowers the concentration of oxygen, which reduces the availability of oxygen for the NO_x forming reactions. The main effect is a reduction in NO_x emissions due to the lower temperatures, but water injection also promotes incomplete combustion and thus increases both CO and HC emissions as well as SFC. SFC is increased due to the lower pressures, which promotes lower power. On the other hand, when injected near TDC, ammonia acts as a fuel and slightly increases the combustion temperature with a negligible effect on CO, HC and SFC. In the next section, the chemical effect of water and ammonia will be analyzed too using the artificial inert species method.

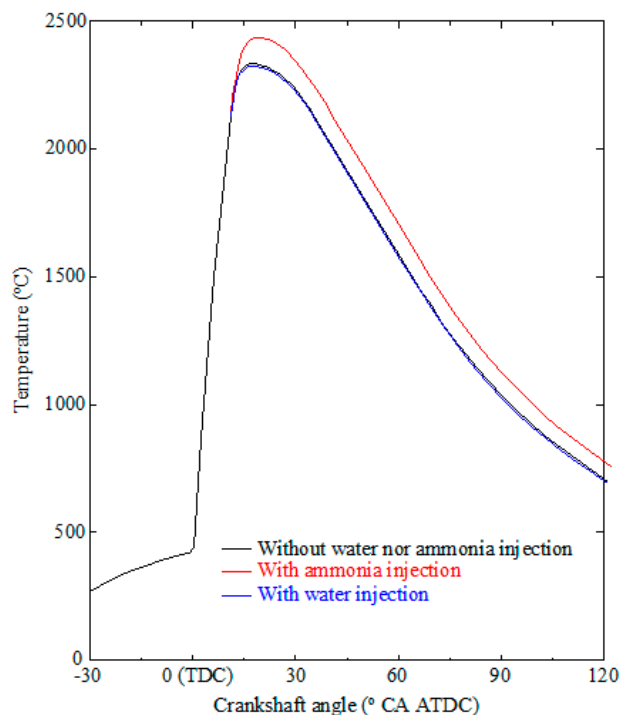


Figure 9. Maximum temperature without water nor ammonia injection; with a 4% ammonia to fuel ratio and an injection timing of -2.1° CA ATDC; water to fuel ratio: 70% and injection timing: -2.1° CA ATDC.

3.2. Artificial Inert Species Method

In this section the so-called artificial inert species method [29–33] is applied to analyze the chemical, thermal, and dilution effects of both ammonia and water injection. The chemical effect is promoted by the chemical reactions. The thermal effect is promoted by the properties, specially the high specific heat capacity of ammonia and water which increases the heat absorption. The dilution effect is promoted by the presence of the additive, which reduces the possibility of reaction between fuel and air.

In the case of water injection, two artificial species were added: inert H_2O and inertAIR. The species inert H_2O has the same properties as water but does not participate in the chemical reactions. On the other hand, the species inertAIR has the same properties as air but does not participate in the chemical reactions. According to this, the difference between the results using water and inert H_2O represents the chemical effect. The dilution effect of water injection is represented by the difference between the results using inertAIR and the base case without water. Finally, the difference between the results using inert H_2O and inertAIR leads to the thermal effect of water injection. Figure 10 illustrates the contribution of thermal, dilution, and chemical effects of water injection for a water injection timing of -2.1° CA ATDC at a 100% load. As can be seen, the chemical effect is negligible. Water injection reduces NO_x by the dilution and, more significantly, thermal effects. The thermal effect is important since water absorbs heat due to its high specific heat capacity. Since water has a higher specific heat capacity than air, the specific heat capacity of the cylinder gases is increased, leading to a reduction in

the in-cylinder temperature and thus to the NO_x emissions. Figure 10 also illustrates the importance of the dilution effect. The presence of water reduces the interaction between fuel and air and thus deteriorate the combustion process.

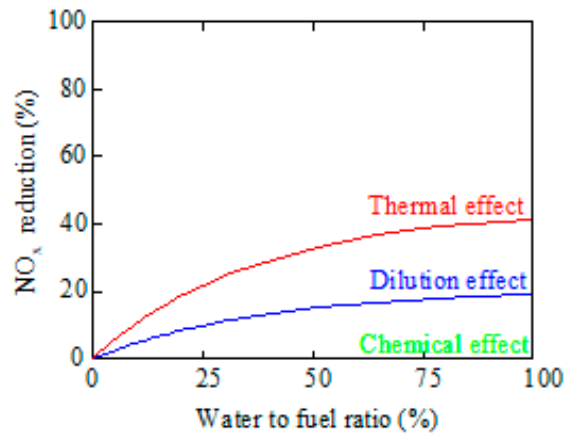


Figure 10. Chemical, thermal, and dilution effects of water injection on NO_x emissions. Water injection timing: -2.1° CA ATDC.

In the case of ammonia injection, two artificial species were added: inertNH₃ and inertAIR. The species inertNH₃ has the same properties as ammonia but does not participate in the chemical reactions. On the other hand, the species inertAIR has the same properties as air but does not participate in the chemical reactions. According to this, the difference of the results using ammonia and inertNH₃ represents the chemical effect of ammonia injection. The dilution effect of ammonia injection is represented by the difference between the results using inertAIR and the base case without ammonia. Finally, the difference between the results using inertNH₃ and inertAIR leads to the thermal effect of ammonia. Figure 11 illustrates the contribution of thermal, dilution, and chemical effects of ammonia injection for an ammonia injection timing of 58.4° CA ATDC at 100% load. As can be seen, the chemical effect is the only one responsible for NO_x reduction, while the thermal and dilution effects are negligible.

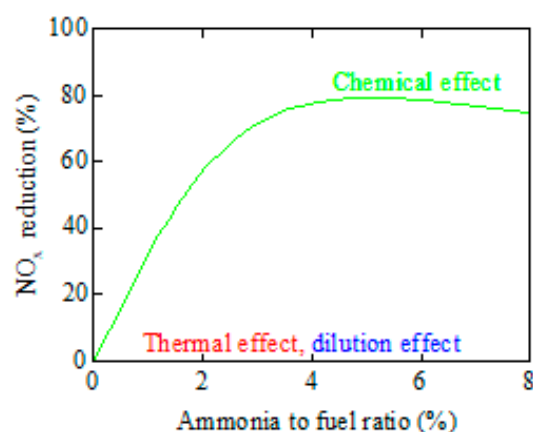


Figure 11. Chemical, thermal, and dilution effects of ammonia injection on NO_x emissions. Ammonia injection timing: 58.4° CA ATDC.

If ammonia is injected near TDC, particularly at -2.1° CA ATDC, the NO_x reduction is noticeably lower, Figure 12. The thermal and dilution effects become more important and the chemical effect is reduced.

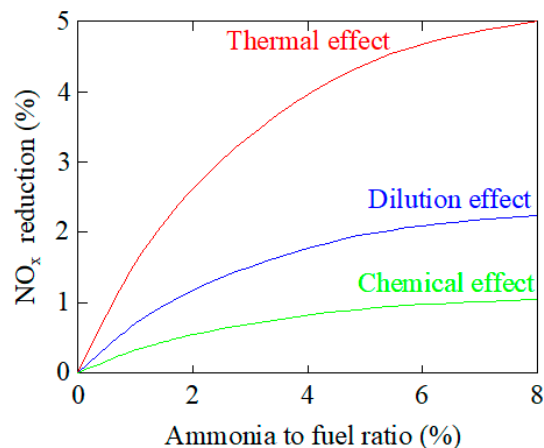


Figure 12. Chemical, thermal, and dilution effects of ammonia injection on NO_x emissions. Ammonia injection timing: -2.1° CA ATDC.

4. Conclusions

This work presents a CFD analysis to study NO_x reduction in a commercial marine engine, the Wärtsilä 6 L 46. The NO_x reduction is based on ammonia injection directly into the cylinder, and this measure was compared with water injection. The so-called artificial inert species method was employed. Inert species with the same properties of water, ammonia, and air were used to characterize the chemical, thermal, and dilution effects of water and ammonia injection.

It was found that the chemical effect using ammonia injection is extremely dependent on the injection timing. The optimum NO_x reduction using ammonia is obtained when this is injected during the expansion stroke, leading to a significant chemical effect, and negligible thermal and dilution effects. The optimum NO_x reduction using water is obtained when this is injected near TDC. Injected near TDC, water promotes NO_x reduction by the dilution and, more significantly, the thermal effect. If ammonia is injected near TDC, the thermal and dilution effects become more significant but the global NO_x reduction is noticeably lower than the values obtained when using water.

Author Contributions: Conceptualization, M.I.L.G. and C.G.R.V.; methodology, M.I.L.G. and C.G.R.V.; software, M.I.L.G. and C.G.R.V.; validation, M.I.L.G. and C.G.R.V.; formal analysis, M.I.L.G. and L.C.-S.; investigation, M.I.L.G. and C.G.R.V.; resources, M.I.L.G. and C.G.R.V.; writing—original draft preparation, M.I.L.G. and L.C.-S.; writing—review and editing, M.I.L.G. and L.C.-S. All authors have read and agreed to the published version of the manuscript.

Funding: This research received no external funding.

Acknowledgments: The authors would like to express their gratitude to Talleres Pineiro S.L., sale and repair of marine engines, as well as to Norplan Engineering S.L.

Conflicts of Interest: The authors declare no conflict of interest.

References

1. Ammar, N.R.; Seddiek, I.S. Eco-environmental analysis of ship emission control methods: Case study RO-RO cargo vessel. *Ocean Eng.* **2017**, *137*, 166–173. [[CrossRef](#)]
2. Seddiek, I.S.; ElGohary, M.M.; Ammar, N.R. The hydrogen-fuelled internal combustion engine for marine application with a case study. *Brodogradnja* **2015**, *66*, 23–38.
3. ElGohary, M.M.; Seddiek, I.S. Utilization of alternative marine fuels for gas turbine power plant onboard ships. *Int. J. Naval Archit. Ocean Eng.* **2013**, *5*, 21–32. [[CrossRef](#)]
4. Lamas, M.I.; Rodríguez, C.G.; Telmo, J.; Rodríguez, J.D. Numerical analysis of emissions from marine engines using alternative fuels. *Polish Marit. Res.* **2015**, *22*, 48–52. [[CrossRef](#)]
5. Kuiken, K. *Diesel Engines for Ship Propulsion and Power Plants*, 3rd ed.; Target Global Energy Training: The Netherlands, 2017.

6. Di Sarli, V. Stability and emissions of a lean pre-mixed combustor with rich catalytic/lean-burn pilot. *Int. J. Chem. React. Eng.* **2014**, *12*, 77–89. [[CrossRef](#)]
7. Sencic, T.; Mrzljak, V.; Blecich, P.; Bonefacic, I. 2D CFD simulation of water injection strategies in a large marine engine. *J. Mar. Sci. Eng.* **2019**, *7*, 296. [[CrossRef](#)]
8. Lamas, M.I.; Rodríguez, C.G.; Rodríguez, J.D.; Telmo, J. Internal modifications to reduce pollutant emissions from marine engines. A numerical approach. *Int. J. Naval Archit. Mar. Eng.* **2013**, *5*, 493–501. [[CrossRef](#)]
9. Lamas, M.I.; Rodríguez, C.G.; Aas, H.P. Computational fluid dynamics analysis of NO_x and other pollutants in the MAN B&W 7S50MC marine engine and effect of EGR and water addition. *Int. J. Marit. Eng.* **2013**, *155*, A81–A88.
10. Puskar, M.; Bigos, P.; Balazikova, M.; Petkova, V. The measurement method solving the problems of engine output characteristics caused by change in atmospheric conditions on the principle of the theory of optimal temperature range of exhaust system. *Meas. J. Int. Meas. Confed.* **2013**, *46*, 467–475. [[CrossRef](#)]
11. Rota, R.; Zanoelo, E.F.; Antos, D.; Morbidelli, M.; Carra, S. Analysis of the thermal DeNO_x process at high partial pressure of reactants. *Chem. Eng. Sci.* **2000**, *55*, 1041–1051. [[CrossRef](#)]
12. Glarborg, P.; Dam-Johansen, K.; Miller, J.A.; Kee, R.J.; Coltrin, M.E. Modeling the thermal DeNO_x process in flow reactors. Surface effects and nitrous oxide formation. *Int. J. Chem. Kinet.* **1994**, *26*, 421–436. [[CrossRef](#)]
13. Rota, R.; Antos, D.; Zanoelo, E.F.; Morbidelli, M. Experimental and modeling analysis of the NO_xOUT process. *Chem. Eng. Sci.* **2002**, *57*, 27–38. [[CrossRef](#)]
14. Birkhold, F.; Meingast, U.; Wassermann, P. *Analysis of the Injection of Urea-Water-Solution for Automotive SCR DeNO_x-Systems: Modeling of Two-Phase Flow and Spray/Wall Interaction*; SAE Technical Paper 2006-01-0643; SAE International: Warrendale, PA, USA, 2006. [[CrossRef](#)]
15. Javed, M.T.; Irfan, N.; Gibbs, B.M. Control of combustion-generated nitrogen oxides by selective non-catalytic reduction. *J. Environ. Manag.* **2007**, *83*, 251–289. [[CrossRef](#)] [[PubMed](#)]
16. Caton, J.A.; Xia, Z. The selective non-catalytic removal (SNCR) of nitric oxides from engine exhaust streams: Comparison of three processes. *Trans. ASME* **2004**, *126*, 234–240. [[CrossRef](#)]
17. Miller, J.A.; Bowman, C. Mechanism and modeling of nitrogen chemistry in combustion. *Prog. Energy Combust. Sci.* **1989**, *15*, 287–338. [[CrossRef](#)]
18. Lyon, R.K. Method for the Reduction of the Concentration of NO in Combustion Effluents Using Ammonia. U.S. Patent 3,900,554, 19 August 1975.
19. Woodyard, D. *Pounder's Marine Engines and Gas Turbines*, 9th ed.; Elsevier: Oxford, UK, 2009.
20. Kimball-Linne, M.A.; Hanson, R.K. Combustion-driven flow reactor studies of thermal DeNO_x reaction kinetics. *Combust. Flame* **1986**, *64*, 337–351. [[CrossRef](#)]
21. Lyon, R.K.; Benn, D. Kinetics of the NO-NH₃-O₂ reaction. *Symp. Combust.* **1979**, *17*, 601–610. [[CrossRef](#)]
22. Kasuya, F.; Glarborg, P.; Johnsson, J.E.; Dam-Johansen, K. The thermal DeNO_x process: Influence of partial pressures and temperature. *Chem. Eng. Sci.* **1995**, *50*, 1455–1466. [[CrossRef](#)]
23. Miyamoto, N.; Ogawa, H.; Wang, J.; Shudo, T.; Yamazaki, K. Diesel NO_x reduction with ammonium deoxidizing agents directly injected into the cylinder. *Int. J. Veh. Des.* **1995**, *16*, 71–79. [[CrossRef](#)]
24. Nam, C.M.; Gibbs, B.M. Selective non-catalytic reduction of NO_x under diesel engine conditions. *Proc. Combust. Inst.* **2000**, *28*, 1203–1209. [[CrossRef](#)]
25. Nam, C.M.; Gibbs, B.M. Application of the thermal DeNO_x process to diesel engine DeNO_x: An experimental and kinetic modelling study. *Fuel* **2002**, *81*, 1359–1367. [[CrossRef](#)]
26. Larbi, N.; Bessrou, J. Measurement and simulation of pollutant emissions from marine diesel combustion engine and their reduction by ammonia injection. *Adv. Mech. Eng.* **2010**, *41*, 898–906. [[CrossRef](#)]
27. Heywood, J. *Internal Combustion Engine Fundamentals*, 2nd ed.; McGraw-Hill Education: New York, NY, USA, 2018.
28. Lesmana, H.; Zhang, Z.; Li, X.; Zhu, M.; Xu, X.; Zhang, D. NH₃ as a transport fuel in internal combustion engines: A technical review. *J. Energy Resour. Technol.* **2019**, *141*, 070703–070714. [[CrossRef](#)]
29. Guo, H.; Neill, W.S. The effect of hydrogen addition on combustion and emission characteristics of an n-heptane fueled HCCI engine. *Int. J. Hydrog. Energy* **2013**, *38*, 11429–11437. [[CrossRef](#)]
30. Voshtani, S.; Reyhanian, M.; Ehteram, M.; Hosseini, V. Investigating various effects of reformer gas enrichment on a natural gas-fueled HCCI combustion engine. *Int. J. Hydrog. Energy* **2014**, *39*, 19799–19809. [[CrossRef](#)]
31. Neshat, E.; Saray, R.K.; Hosseini, V. Effect of reformer gas blending on homogeneous charge compression ignition combustion of primary reference fuels using multi zone model and semi detailed chemical-kinetic mechanism. *Appl. Energy* **2016**, *179*, 463–478. [[CrossRef](#)]

32. Neshat, E.; Saray, R.K.; Parsa, S. Numerical analysis of the effects of reformer gas on supercharged n-heptane HCCI combustion. *Fuel* **2017**, *200*, 488–498. [[CrossRef](#)]
33. Neshat, E.; Bajestani, A.V.; Honnery, D. Advanced numerical analyses on thermal, chemical and dilution effects of water addition on diesel engine performance and emissions utilizing artificial inert species. *Fuel* **2019**, *242*, 596–606. [[CrossRef](#)]
34. Lamas, M.I.; Rodríguez, C.G.; Rebolledo, J.M. Numerical model to study the valve overlap period in the Wärtsilä 6L46 four-stroke marine engine. *Polish Marit. Res.* **2012**, *19*, 31–37. [[CrossRef](#)]
35. Lamas, M.I.; Rodríguez, C.G. Numerical model to study the combustion process and emissions in the Wärtsilä 6L 46 four-stroke marine engine. *Polish Marit. Res.* **2013**, *20*, 61–66. [[CrossRef](#)]
36. Polanowski, S.; Pawletko, R.; Witkowski, K. Influence of the indicator channel and indicator valve on the heat release characteristics of medium speed marine diesel engines. *Key Eng. Mater.* **2014**, *588*, 149–156. [[CrossRef](#)]
37. Ricart, L.M.; Xin, J.; Bower, G.R.; Reitz, R.D. *In-Cylinder Measurement and Modeling of Liquid Fuel Spray Penetration in a Heavy-Duty Diesel Engine*; SAE Technical Paper 971591; SAE International: Warrendale, PA, USA, 1997. [[CrossRef](#)]
38. Dukowicz, J.K. A particle-fluid numerical model for liquid sprays. *J. Comput. Phys.* **1980**, *35*, 229–253. [[CrossRef](#)]
39. Weber, J. *Optimization Methods for the Mixture Formation and Combustion Process in Diesel Engines*, 1st ed.; Cuvillier Verlag: Göttingen, Germany, 2008.
40. Sigurdsson, E.; Ingvorsen, K.M.; Jensen, M.V.; Mayer, S.; Matlok, S.; Walther, J.H. Numerical analysis of the scavenge flow and convective heat transfer in large two-stroke marine diesel engines. *Appl. Energy* **2014**, *123*, 37–46. [[CrossRef](#)]
41. Taylor, C.F. *The Internal Combustion Engine in Theory and Practice*, 2nd ed; MIT Press: Cambridge, MA, USA, 1985.
42. Ra, Y.; Reitz, R. A reduced chemical kinetic model for IC engine combustion simulations with primary reference fuels. *Combust. Flame* **2008**, *155*, 713–738. [[CrossRef](#)]
43. Lamas, M.; Rodriguez, C.G. Numerical model to analyze NOx reduction by ammonia injection in diesel-hydrogen engines. *Int. J. Hydrog. Energy* **2017**, *42*, 26132–26141. [[CrossRef](#)]
44. Lamas, M.I.; de Dios Rodriguez, J.; Castro-Santos, L.; Carral, L.M. Effect of multiple injection strategies on emissions and performance in the Wärtsilä 6L 46 marine engine. A numerical approach. *J. Clean. Prod.* **2019**, *206*, 1–10. [[CrossRef](#)]
45. Sher, E. *Handbook of Air Pollution from Internal Combustion Engines*; Academic Press: Boston, MA, USA, 1998.
46. Lapuerta, M.; Hernández, J.; Armas, O. *Kinetic Modelling of Gaseous Emissions in a Diesel Engine*; SAE Technical Paper 2000-01-2939; SAE International: Warrendale, PA, USA, 2000. [[CrossRef](#)]
47. Yang, H.; Krishnan, S.R.; Srinivasan, K.K.; Midkiff, K.C. Modeling of NOx emissions using a super-extended Zeldovich mechanism. In Proceedings of the ICEF03 2003 Fall Technical Conference of the ASME Internal Combustion Engine Division, Erie, PA, USA, 7–10 September 2003.
48. Zeldovich, Y.B.; Sadochnikov, D.A.; Kamenetskii, F. *Oxidation of Nitrogen in Combustion*; Institute of Chemical Physics: Moscow-Leningrad, Russia, 1947.
49. Lavoie, G.A.; Heywood, J.B.; Keck, J.C. Experimental and theoretical investigation of nitric oxide formation in internal combustion engines. *Combust. Sci. Technol.* **1970**, *1*, 313–326. [[CrossRef](#)]
50. Lamas, M.I.; Rodriguez, C.G. NOx reduction in diesel-hydrogen engines using different strategies of ammonia injection. *Energies* **2019**, *12*, 1255. [[CrossRef](#)]
51. Miller, J.A.; Glarborg, P. Modeling the formation of N2O and NO2 in the thermal DeNOx process. *Springer Ser. Chem. Phys.* **1996**, *61*, 318–333.
52. Lamas, M.I.; Rodriguez, C.G.; Rodriguez, J.D.; Telmo, J. Computational fluid dynamics of NOx reduction by ammonia injection in the MAN B&W 7S50MC marine engine. *Int. J. Marit. Eng.* **2014**, *156*, A213–A220. [[CrossRef](#)]

